



Search for the suppressed decays $B^+ \rightarrow K^+K^+\pi^-$ and $B^+ \rightarrow \pi^+\pi^+K^-$

The LHCb Collaboration



ARTICLE INFO

Article history:

Received 8 August 2016

Received in revised form 10 November 2016

Accepted 16 November 2016

Available online 2 December 2016

Editor: L. Rolandi

ABSTRACT

A search is made for the highly-suppressed B meson decays $B^+ \rightarrow K^+K^+\pi^-$ and $B^+ \rightarrow \pi^+\pi^+K^-$ using a data sample corresponding to an integrated luminosity of 3.0 fb^{-1} collected by the LHCb experiment in proton–proton collisions at centre-of-mass energies of 7 and 8 TeV. No evidence is found for the decays, and upper limits at 90% confidence level are determined to be $\mathcal{B}(B^+ \rightarrow K^+K^+\pi^-) < 1.1 \times 10^{-8}$ and $\mathcal{B}(B^+ \rightarrow \pi^+\pi^+K^-) < 4.6 \times 10^{-8}$.

© 2016 The Author. Published by Elsevier B.V. This is an open access article under the CC BY license (<http://creativecommons.org/licenses/by/4.0/>). Funded by SCOAP³.

1. Introduction

Transitions of the type $b \rightarrow s\bar{s}$ and $b \rightarrow d\bar{s}$ are rare in the Standard Model (SM) [1,2]. The calculation of the $b \rightarrow s\bar{s}$ amplitude results in branching fractions of at most $\mathcal{O}(10^{-11})$, the exact value depending on the unknown relative phase between t and c quark contributions in the W^\pm -exchange box [3], as shown in Fig. 1. The magnitude of the $b \rightarrow d\bar{s}$ amplitude is expected to be even smaller due to the relative $|V_{td}/V_{ts}|$ factor, leading to predicted branching fractions of $\mathcal{O}(10^{-14})$ [4].

Physics beyond the Standard Model (BSM) could result in enhanced branching fractions that can be detected at current experiments. Theoretical models that have been investigated include the Minimal Supersymmetric Standard Model with and without R-Parity Violation, variations of the two Higgs doublet model, and extensions of the SM where an additional flavour changing Z' neutral boson is present [3,4]. In these SM extensions, for certain plausible values of the model parameters, $b \rightarrow s\bar{s}$ and $b \rightarrow d\bar{s}$ transitions may lead to branching fractions of up to 10^{-8} and 10^{-7} , respectively. It has been suggested by these theoretical studies that the most suitable three-body decay modes to see the effects of BSM physics in such transitions are the $B^+ \rightarrow K^+K^+\pi^-$ and $B^+ \rightarrow \pi^+\pi^+K^-$ decays, where two particles in the final state have the same flavour and charge.¹

An upper limit of 1.29×10^{-4} at 90% confidence level on the branching fraction for the $B^+ \rightarrow \pi^+\pi^+K^-$ decay was first determined by OPAL [5]. Improvements in sensitivity were obtained by the e^+e^- B -factories, and currently the 90% confidence level upper limits for $B^+ \rightarrow K^+K^+\pi^-$ and $B^+ \rightarrow \pi^+\pi^+K^-$ decays are 1.6×10^{-7} and 9.5×10^{-7} , respectively [6–8].

This paper reports on the search for the suppressed decays $B^+ \rightarrow K^+K^+\pi^-$ and $B^+ \rightarrow \pi^+\pi^+K^-$ using data samples corresponding to 1.0 and 2.0 fb^{-1} collected by LHCb at $\sqrt{s} = 7$ and 8 TeV, respectively. The corresponding unsuppressed decays $B^+ \rightarrow K^+K^-\pi^+$ and $B^+ \rightarrow \pi^+\pi^-K^+$ are used for normalisation.

2. Detector and simulation

The LHCb detector [9,10] is a single-arm forward spectrometer covering the pseudorapidity range $2 < \eta < 5$, designed for the study of particles containing b or c quarks. The detector includes a high-precision tracking system consisting of a silicon-strip vertex detector surrounding the pp interaction region, a large-area silicon-strip detector located upstream of a dipole magnet with a bending power of about 4 Tm, and three stations of silicon-strip detectors and straw drift tubes placed downstream of the magnet. The polarity of the dipole magnet is reversed periodically throughout data-taking. The configuration with the magnetic field vertically upwards (downwards) bends positively (negatively) charged particles in the horizontal plane towards the centre of the LHC. The tracking system provides a measurement of momentum, p , of charged particles with a relative uncertainty that varies from 0.5% at low momentum to 1.0% at 200 GeV/c. The impact parameter (IP) is the minimum distance of a track to a primary vertex (PV) and is measured with a resolution of $(15 + 29/p_T)\mu\text{m}$, where p_T is the component of the momentum transverse to the beam, in GeV/c. Different types of charged hadrons are distinguished using information from two ring-imaging Cherenkov (RICH) detectors [11]. Photons, electrons and hadrons are identified by a calorimeter system consisting of scintillating-pad and preshower detectors, an electromagnetic calorimeter and a hadronic calorimeter. Muons are identified by a system composed of alternating layers of iron and multiwire proportional chambers [12].

¹ The inclusion of charge-conjugate decays is implied throughout.

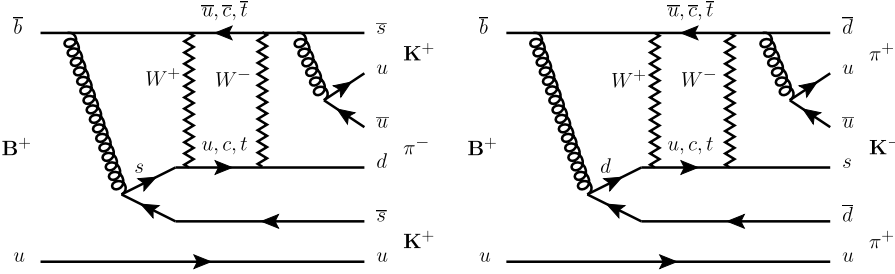


Fig. 1. Main SM diagrams for the suppressed decays (left) $B^+ \rightarrow K^+K^+\pi^-$ and (right) $B^+ \rightarrow \pi^+\pi^+K^-$.

The online event selection is performed by a trigger [13], which consists of a hardware stage, based on information from the calorimeter and muon systems, followed by a software stage, which applies a full event reconstruction. At the hardware stage, the candidates are triggered either one of the particles from the b candidate decay depositing a transverse energy of at least 3500 MeV in the calorimeter, or by other activity in the event, mainly associated with the decay products of the other b hadron produced in the pp primary interaction.

Simulated $B^+ \rightarrow K^+K^\pm\pi^\mp$ and $B^+ \rightarrow \pi^+\pi^\pm K^\mp$ decays, generated uniformly in phase space, are used to optimize the suppressed signal selections and to evaluate the ratios of the efficiencies for each suppressed decay mode relative to their corresponding unsuppressed decay modes. In the simulation, pp collisions are generated using Pythia 8 [14,15] with a specific LHCb configuration [16]. Decays of hadronic particles are described by EvtGen [17] in which final state radiation is generated by Photos [18]. The interaction of the generated particles with the detector and its response are implemented using the Geant4 toolkit [19] as described in Ref. [20].

3. Event selection

The candidate $B^+ \rightarrow K^+K^\pm\pi^\mp$ and $B^+ \rightarrow \pi^+\pi^\pm K^\mp$ decays are reconstructed using three charged tracks with mass hypotheses and total charge consistent with the decay. The final state particles are required to have a good track fit with a reduced chi-square $\chi^2/\text{ndf} < 3$. All three tracks must have momentum $p > 1500 \text{ MeV}/c$, transverse momentum $p_T > 100 \text{ MeV}/c$, and $\chi^2_{\text{IP}} > 1$ with respect to all PVs in the event. The quantity χ^2_{IP} is defined as the difference between the vertex-fit χ^2 of the PV reconstructed with and without the considered track. Combinatorial backgrounds are suppressed by requiring that the scalar sum of the p_T of the tracks is greater than $4500 \text{ MeV}/c$ and the sum of the tracks' $\chi^2_{\text{IP}} > 200$. The track with the highest p_T must have $\text{IP} > 0.05 \text{ mm}$. The second highest track p_T is required to be greater than $900 \text{ MeV}/c$. The maximum distance of closest approach between tracks has to be less than 0.2 mm .

The information from the RICH, calorimeter and muon systems is used for particle identification (PID). Muons are rejected by a veto applied to each track. Loose kaon and pion PID is required for the remaining charged tracks to reduce the number of wrong combinations before forming a B^+ candidate.

The reconstructed B^+ candidates are required to have an invariant mass in the range $5080\text{--}5480 \text{ MeV}/c^2$, $p_T > 1700 \text{ MeV}/c$, $\chi^2_{\text{IP}} < 10$, vertex fit $\chi^2/\text{ndf} < 12$, distance between the PV and the decay point (or secondary vertex, SV) greater than 3 mm , and a significant displacement between primary and secondary vertex, with the three dimensional χ^2 -distance between the two greater than 700 . When more than one PV is reconstructed, the one with the minimum χ^2_{IP} for the B^+ candidate is chosen. The cosine of the angle θ_f between the reconstructed momentum of the B^+ candidate

and the B^+ candidate flight direction is required to be $\cos\theta_f > 0.99998$. The pointing variable $\theta_p \equiv P_B \sin\theta_f / (P_B \sin\theta_f + \sum_i q_{T,i})$ is required to be less than 0.05 , where P_B is the total momentum of the three-particle final state and $\sum_i q_{T,i}$ is the sum of the transverse momenta of the three tracks with respect to the momentum direction of the B^+ candidate. These requirements remove additional combinatorial background and partially reconstructed b hadron decays.

Depending on its charge and the polarity of the dipole magnet, a charged particle traversing the magnetic field can be bent horizontally into or out of the detector acceptance. To minimise charge-dependent differences in the reconstruction efficiencies for the signal or normalisation channels caused by the magnetic field, an additional criterion is placed on the x and z components² of the B^+ candidate momentum such that $|p_x| \leq 0.317 \times (p_z - 2400 \text{ MeV}/c)$ [21], which ensures that tracks of both charges are well contained in the detector acceptance.

A B^+ candidate is rejected if the invariant mass formed from two of the charged tracks with opposite charge is within $25 \text{ MeV}/c^2$ of the D^0 mass. The D^0 veto suppresses possible background from $B^+ \rightarrow D^0 h^+$ decays. Backgrounds from $B^0 \rightarrow D^- h^+$ decays are found to be negligible. For $B^+ \rightarrow \pi^+\pi^-K^+$ decays only, an additional invariant mass criterion of $|3104 \text{ MeV}/c^2 - m_{\pi^+\pi^-K^+}| > 20 \text{ MeV}/c^2$ is required to eliminate contamination $J/\psi \rightarrow \mu^+\mu^-$, where the muons are misidentified as pions, and from $J/\psi \rightarrow \pi^+\pi^-$.

The reconstructed candidates that meet the above criteria are filtered using a boosted decision tree (BDT) algorithm [22,23]. The BDT is trained with a sample of simulated signal candidates and a background sample of data candidates taken from the B^+ candidate invariant mass sideband above $5400 \text{ MeV}/c^2$, which is dominated by combinatorial background. The training is performed separately for events that have been triggered by information from the signal decay only and for events that have been triggered by other particles. This is required as the two trigger scenarios have different sensitivities to the signal and background. The input variables are chosen to produce the best discrimination and to minimise the dependence of the BDT on the mass of the B^+ candidate, the PID variables and on the kinematic configuration of the B^+ candidate parametrised in the Dalitz plane. The twelve variables used by the BDT are: the B^+ candidate p_T ; the flight distance between the PV and B^+ candidate SV; the angle θ_f ; the B^+ candidate pointing angle θ_p ; the p_T of the track with the lowest p_T ; the sum of the tracks' p_T ; the sum of the χ^2_{IP} of the three tracks; the IP of the track with the highest p_T , with respect to the PV; the momentum p of each of the three tracks; and the χ^2_{IP} of the track reconstructed with the π hypothesis for $B^+ \rightarrow K^+K^\pm\pi^\mp$ decays or the K hypothesis for $B^+ \rightarrow \pi^+\pi^\pm K^\mp$ decays. The same set of variables is found to result in a robust

² In the LHCb right handed coordinate system, the z -axis points from the interaction point into the experiment and the y -axis is vertical, pointing upwards.

multivariate classifier for the four decay channels under consideration.

A figure of merit $FOM \equiv \epsilon/(0.5 \times N_\sigma + \sqrt{N_B})$, is used to identify the optimal BDT selection criteria. Here ϵ is the simulated signal selection efficiency, N_B is the number of background events that pass the selection and have a mass in a ± 50 MeV/c 2 window around the B^\pm mass [24], and N_σ is the required significance, expressed in terms of standard deviations from the hypothesis of a null signal [25]. The quantity FOM is optimized with $N_\sigma = 5$, but the final result is robust against changes of one or two units in N_σ . For events that pass the selection criteria described above, the optimal BDT selection criterion for $B^+ \rightarrow K^+ K^+ \pi^-$ results in 85% of the simulated signal events being accepted and 71% of the background events rejected. For $B^+ \rightarrow \pi^+ \pi^+ K^-$, 67% of the simulated signal events are accepted and 91% of the background events are rejected.

After the BDT selection criterion has been applied, each track is required to pass PID criteria. Each track has a probability to be a kaon and a probability to be a pion, leading in total to six possible PID assignments for a B^+ candidate. The same FOM optimisation described above is performed for each of the six cases in turn, starting with the track with the highest p_T . After the application of these criteria, less than 2–4% have more than one candidate, depending on the decay mode. For these multiple candidate events, one candidate is chosen at random and the others discarded.

The efficiencies of all the selection requirements are calculated with simulated events. The PID efficiency for hadrons is determined from data using large calibration samples of $D^{*+} \rightarrow D^0 (\rightarrow K^-\pi^+)\pi^+$ decays. The PID efficiencies in the simulated sample are corrected by reweighting the calibration sample to match the momentum and the pseudorapidity distributions of the final state particles in the signal decay and the multiplicity of tracks in the event. The effective kaon and pion PID efficiencies in this analysis are approximately 90% and 80%, respectively. The rates for misidentifying a kaon as a pion or a pion as a kaon are less than 0.1%.

After all selection criteria have been applied, the ratio of the $B^+ \rightarrow K^+ K^+ \pi^+$ to $B^+ \rightarrow K^+ K^+ \pi^-$ selection efficiencies, weighted by the integrated luminosity taken with different magnet polarities and beam energy, is 1.00 ± 0.02 , while the ratio of the $B^+ \rightarrow \pi^+ \pi^- K^+$ to $B^+ \rightarrow \pi^+ \pi^+ K^-$ selection efficiencies is 0.97 ± 0.01 . The quoted uncertainties are statistical only and are due to the limited simulation sample size. For each of the four modes, the selection efficiency across the Dalitz plane is constant with a relative variation of less than 9%.

4. Determination of the signal yields

Signal yields are determined from simultaneous, unbinned and extended maximum likelihood fits to the invariant mass distributions $m_{h^+ h^\pm h^\mp}$ of the suppressed and unsuppressed decays, where h and h' denote π or K . Separate fits are made for $B^+ \rightarrow K^+ K^+ \pi^-$ and $B^+ \rightarrow K^+ K^+ \pi^+$ decays, and for $B^+ \rightarrow \pi^+ \pi^+ K^-$ and $B^+ \rightarrow \pi^+ \pi^- K^+$ decays.

The signal component for both the suppressed and unsuppressed decays is parameterised as the sum of a Gaussian function and a Crystal Ball function [26]. The values of the signal function parameters are constrained to be the same for both the suppressed and unsuppressed signal components.

For all decay modes, the combinatorial background is parameterised with an exponential function. Partially reconstructed backgrounds, largely due to B decays with four or more particles in the final state, where one or more particles are not reconstructed, appear predominantly at $m_{h^+ h^\pm h^\mp}$ masses below 5150 MeV/c 2 and are modelled with an ARGUS function [27] convolved with a Gaus-

sian resolution function. In the case of the suppressed $B^+ \rightarrow \pi^+ \pi^+ K^-$ mode, an additional component, modelled in the same way, is used to account for B_s^0 four-body decays such as $B_s^0 \rightarrow D_s^- \pi^+$, with $D_s^- \rightarrow K^- \pi^+ \pi^-$, where one of the decay particles is not reconstructed. These appear at $m_{h^+ h^\pm h^\mp}$ masses below 5250 MeV/c 2 . The slope parameter of this ARGUS function is fixed from a fit to simulated decays. The signal yields, background yields, and all signal and background parameters (apart from the fixed slope parameter of the $B_s^0 \rightarrow D_s^- \pi^+$ component) are allowed to float in the fit.

To investigate the presence of any peaking background in the signal mass region, a total of 350 million events from 200 B , B_s^0 , Λ_b^0 , and Ξ_b decays are simulated and reconstructed using the same selection criteria used for the signal decay modes. In addition, the data are divided into two samples, above and below the signal mass region $5230 < m_{h^+ h^\pm h^\mp} < 5320$ MeV/c 2 . The Dalitz plot distributions in each sample are studied to identify any resonances that might be present in the signal region. There is no evidence for any peaking background in the signal mass region.

The performance of the fit procedure is tested by creating ensembles of simulated datasets generated from the functions fitted to the data. A large number of datasets is generated and fits are performed with the number of signal and background events left free to fluctuate according to a Poisson distribution. The fit biases on the signal yields extracted from the pseudoexperiments are 0.05 ± 0.10 and -0.48 ± 0.15 events for the $B^+ \rightarrow K^+ K^+ \pi^-$ and $B^+ \rightarrow \pi^+ \pi^+ K^-$ decays, respectively, where the uncertainty is statistical only.

Fig. 2 shows the fit to the $B^+ \rightarrow K^+ K^+ \pi^-$ and $B^+ \rightarrow K^+ K^+ \pi^+$ decay candidates. The signal yields are -7.2 ± 4.6 and 955 ± 75 for $B^+ \rightarrow K^+ K^+ \pi^-$ and $B^+ \rightarrow K^+ K^+ \pi^+$ respectively. **Fig. 3** shows the fit to the $B^+ \rightarrow \pi^+ \pi^+ K^-$ and $B^+ \rightarrow \pi^+ \pi^- K^+$ decay candidates. The signal yields are 2.7 ± 10.0 and $24\,044 \pm 193$ for $B^+ \rightarrow \pi^+ \pi^+ K^-$ and $B^+ \rightarrow \pi^+ \pi^- K^+$, respectively. The $B^+ \rightarrow K^+ K^+ \pi^-$ and $B^+ \rightarrow \pi^+ \pi^+ K^-$ signal yields have been corrected for the fit bias introduced by the fitting procedure.

The branching fractions of the suppressed decays are calculated using

$$\mathcal{B}_{\text{sup}} = \frac{N_{\text{sig}}^{\text{sup}}}{N_{\text{sig}}^{\text{unsup}}} \times \frac{\epsilon^{\text{unsup}}}{\epsilon^{\text{sup}}} \times \mathcal{B}_{\text{unsup}}, \quad (1)$$

where $N_{\text{sig}}^{\text{unsup}}$ and $N_{\text{sig}}^{\text{sup}}$ are the numbers of fitted signal events for the unsuppressed and suppressed modes (corrected for fit bias), while ϵ^{unsup} and ϵ^{sup} are the selection efficiencies calculated from simulated events and corrected for differences in selection efficiency between simulation and data [28]. Finally, $\mathcal{B}_{\text{unsup}}$ is the known branching fraction for the unsuppressed reference mode [24].

5. Systematic uncertainties

The measurements of the branching fractions of the suppressed modes depend on the ratios of suppressed to unsuppressed signal yields and selection efficiencies. Since the final state is the same, apart from the charge assignment, the ratio of unsuppressed and suppressed selection efficiencies is close to unity, and most of the systematic uncertainties cancel.

The main systematic uncertainties on the branching fractions are due to the unsuppressed branching fraction uncertainties, PID charge dependence, discrepancies in PID between data and simulated events, fit biases, alternative mass fit models, simulated event statistics, and assumptions concerning the Dalitz plot distributions.

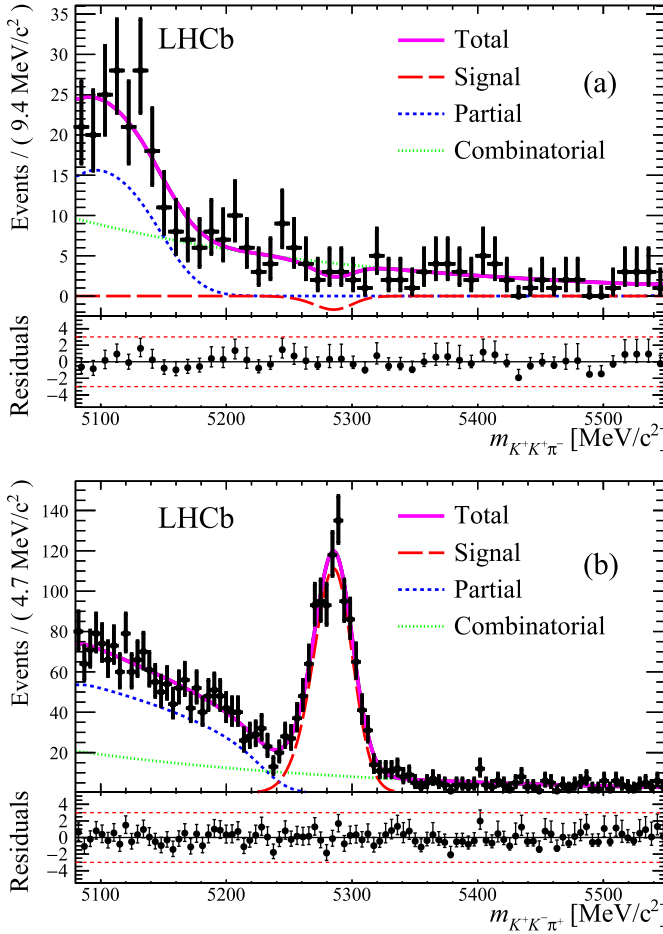


Fig. 2. Invariant mass spectra of (a) $B^+ \rightarrow K^+K^+\pi^-$ and (b) $B^+ \rightarrow K^+K^-\pi^+$ candidates, with the results of the unbinned extended maximum likelihood fits overlaid. The dashed (blue) line represents the partially reconstructed background, the dotted (green) line the combinatorial background, the long dashed (red) line is the signal, and the solid (magenta) line the total. Residual differences between data and the fits are shown below the mass plots in units of standard deviation. (For interpretation of the references to colour in this figure legend, the reader is referred to the web version of this article.)

The uncertainties on the known $B^+ \rightarrow K^+K^-\pi^+$ and $B^+ \rightarrow \pi^+\pi^-K^+$ branching fractions result in systematic uncertainties of 0.53×10^{-8} and 0.32×10^{-9} , respectively [29–31]. Systematic uncertainties of 0.04×10^{-8} and 0.03×10^{-9} are assigned to the $B^+ \rightarrow K^+K^-\pi^+$ and $B^+ \rightarrow \pi^+\pi^-K^+$ decay modes, respectively, to account for the effect of limited simulated events available to determine the reconstruction efficiencies.

Studies have shown a small PID dependence on the track charge with differences in efficiency below 0.2% for π^\pm and below 0.4% for K^\pm . Systematic uncertainties of 0.04×10^{-8} are assigned to both the $B^+ \rightarrow K^+K^-\pi^+$ and the $B^+ \rightarrow \pi^+\pi^-K^+$ branching fractions, derived from a 0.2% systematic uncertainty per pion and 0.4% per kaon, added linearly. The PID efficiency is extracted from data and systematic uncertainties of 0.09×10^{-8} and 0.11×10^{-9} are applied to $B^+ \rightarrow K^+K^-\pi^-$ and $B^+ \rightarrow \pi^+\pi^-K^+$, respectively, to account for different data-taking conditions.

The process used to determine the selection criteria for the BDT output and the six PID probabilities is validated by changing the order in which the PID criteria are optimized, adjusting the FOM for the predicted suppressed signal yield (using published branching fraction upper limits [6–8]) rather than the signal reconstruction efficiency ϵ , and reweighting the simulation samples to

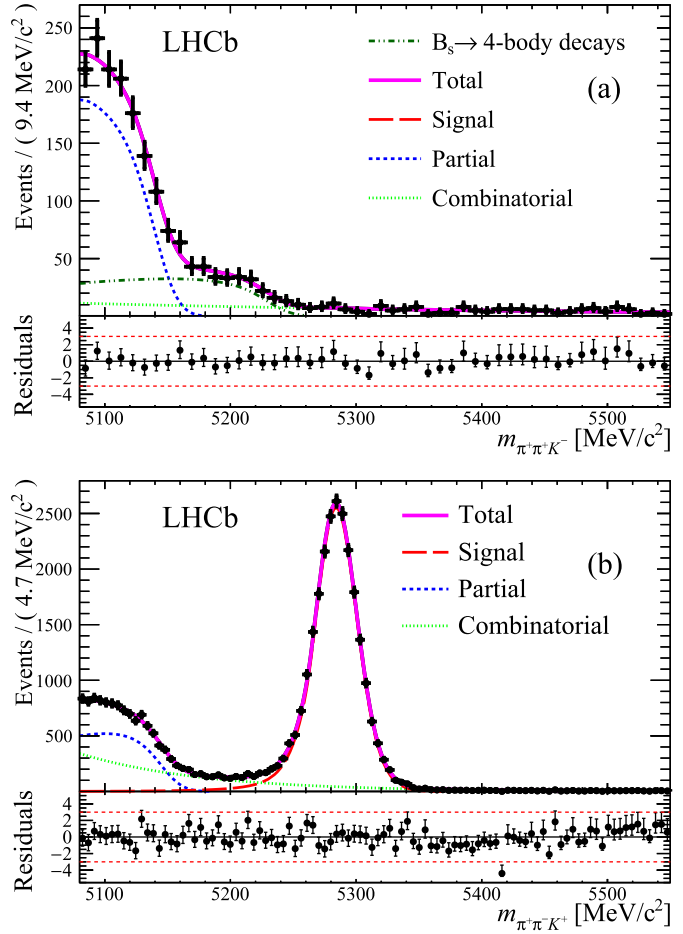


Fig. 3. Invariant mass spectra of (a) $B^+ \rightarrow \pi^+\pi^+K^-$ and (b) $B^+ \rightarrow \pi^+\pi^-K^+$ candidates, with the results of the unbinned extended maximum likelihood fits overlaid. The dashed (blue) line represents the partially reconstructed background, the dotted (green) line the combinatorial background, the long dashed (red) line is the signal, the dot-dash (dark green) line the B_s^0 four-body backgrounds, and the solid (magenta) line the total. Residual differences between data and the fits are shown below the mass plots in units of standard deviation. (For interpretation of the references to colour in this figure legend, the reader is referred to the web version of this article.)

match PID distributions in data [28]. The process is shown to be robust and no systematic uncertainty is applied.

To allow for possible differences in reconstruction efficiency as a function of position in the Dalitz plane due to resonances and interference, simulated events are generated with a distribution of resonances taken from previous published results, which are however only available for the $B^+ \rightarrow \pi^+\pi^-K^+$ decay [29,30]. The average values of the reconstruction efficiencies for the phase-space and resonance-allowed Dalitz plots differ by $(8 \pm 2)\%$, which is taken as the difference between a phase-space and a resonance-allowed distribution for all modes. The resulting uncertainties are 0.15×10^{-8} and 0.22×10^{-9} for $B^+ \rightarrow K^+K^-\pi^-$ and $B^+ \rightarrow \pi^+\pi^-K^+$, respectively.

The fit bias from the ensemble of simulated pseudoexperiments generated from the fit to data is used to correct the signal yield observed in data. The systematic uncertainty on this correction is defined as half the fit bias added in quadrature with the fit bias statistical uncertainty. The systematic uncertainties introduced by this procedure are 0.05×10^{-8} and 0.58×10^{-9} for the $B^+ \rightarrow K^+K^-\pi^-$ and $B^+ \rightarrow \pi^+\pi^-K^+$ branching fractions, respectively.

To understand the impact of the fit model on the results, the components of the default models are changed independently. The

Table 1

Systematic uncertainties on the $B^+ \rightarrow K^+K^+\pi^-$ and $B^+ \rightarrow \pi^+\pi^+K^-$ branching fractions in units of 10^{-8} and 10^{-9} , respectively.

Criteria	$B^+ \rightarrow K^+K^+\pi^-$	$B^+ \rightarrow \pi^+\pi^+K^-$
Simulation statistics	0.04	0.03
PID charge dependence	0.04	0.04
PID discrepancies	0.09	0.11
Dalitz plot efficiencies	0.15	0.22
Fit bias	0.05	0.58
Fit model	0.45	0.29
Subtotal	0.49	0.69
PDG $\mathcal{B}_{\text{unsup}}$ uncertainty [24]	0.53	0.32
Total	0.72	0.76

signal component is replaced with a Crystal Ball function. The slope parameter of the $B_s^0 \rightarrow D_s^-\pi^+$ ARGUS function is allowed to float and the $B_s^0 \rightarrow D_s^-\pi^+$ component is replaced with a bifurcated Gaussian function. The combinatorial background distribution is modelled with a second order polynomial instead of an exponential. Studies of cross-feed from simulated unsuppressed $B^+ \rightarrow h^+h^-h^+$ decays, where the flavour of one or more particles is misidentified, indicate 5.7 ± 2.7 events in the $B^+ \rightarrow K^+K^+\pi^-$ decay mode and 3.1 ± 1.8 events in $B^+ \rightarrow \pi^+\pi^+K^-$ decay mode. The uncertainty is dominated by limited simulation sample size. Cross-feed events are shifted by a minimum of $\sim 40 \text{ MeV}/c^2$ above and below the B mass and the majority of the events do not appear in the signal region. To confirm this, the fit is repeated with two additional Gaussian functions centred around $5240 \text{ MeV}/c^2$ and $5320 \text{ MeV}/c^2$, respectively. As a cross-check, an additional fit is performed with the means and widths of the Gaussian component allowed to vary. The fitted yields are compatible with zero. Systematic uncertainties of 0.45×10^{-8} and 0.29×10^{-9} are assigned for the $B^+ \rightarrow K^+K^+\pi^-$ and $B^+ \rightarrow \pi^+\pi^+K^-$ decays, respectively.

The total systematic uncertainty is determined by adding the individual contributions in quadrature. A summary of the systematic uncertainties is given in Table 1. The total systematic uncertainties are 0.72×10^{-8} and 0.76×10^{-9} for $B^+ \rightarrow K^+K^+\pi^-$ and $B^+ \rightarrow \pi^+\pi^+K^-$, respectively.

6. Results and conclusions

Including all statistical and systematic uncertainties, the ratios of branching fractions are calculated to be

$$\begin{aligned} \frac{\mathcal{B}(B^+ \rightarrow K^+K^+\pi^-)}{\mathcal{B}(B^+ \rightarrow K^+K^-\pi^+)} &= (-7.5 \pm 4.9 \pm 1.0) \times 10^{-3}, \\ \frac{\mathcal{B}(B^+ \rightarrow \pi^+\pi^+K^-)}{\mathcal{B}(B^+ \rightarrow \pi^+\pi^-K^+)} &= (1.1 \pm 4.0 \pm 0.1) \times 10^{-4}, \end{aligned}$$

where the first uncertainties are statistical and the second are systematic. Using the above and the world average of the unsuppressed branching fractions [24] and using Eq. (1), we calculate the branching fractions

$$\begin{aligned} \mathcal{B}(B^+ \rightarrow K^+K^+\pi^-) &= (-3.8 \pm 2.4 \pm 0.5 \pm 0.5) \times 10^{-8}, \\ \mathcal{B}(B^+ \rightarrow \pi^+\pi^+K^-) &= (5.6 \pm 21.0 \pm 0.7 \pm 0.3) \times 10^{-9}, \end{aligned} \quad (2)$$

where the first uncertainties are statistical, the second are systematic without the unsuppressed decay branching fraction uncertainties, and the third are associated with the present knowledge of the $B^+ \rightarrow K^+K^-\pi^+$ and $B^+ \rightarrow \pi^+\pi^-K^+$ branching fractions.

To obtain upper limits on the branching fractions, the frequentist approach of Feldman and Cousins [32] is used to determine 90% and 95% confidence region bands that relate the true values of the branching fractions to the measured numbers of signal

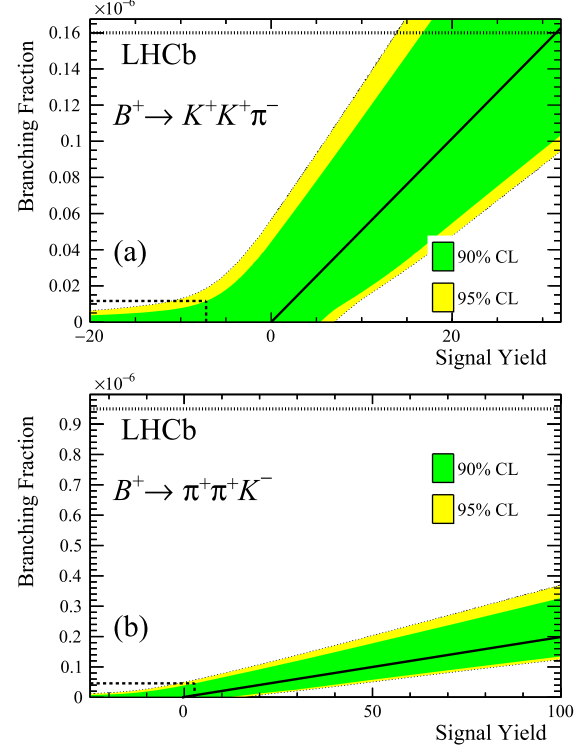


Fig. 4. Feldman–Cousins 90% (green) and 95% (yellow) confidence level (CL) bands for (a) $B^+ \rightarrow K^+K^+\pi^-$ and (b) $B^+ \rightarrow \pi^+\pi^+K^-$, including statistical and systematic uncertainties. The black solid line shows the expected central value of the true branching fraction as a function of the fitted number of signal events. The horizontal dotted lines show the 90% CL upper limits on the branching fractions prior to the present measurement. The dashed lines in the lower left corner of each figure show the equivalent 90% CL upper limits reported in this paper. (For interpretation of the references to colour in this figure legend, the reader is referred to the web version of this article.)

events. These bands are constructed using the results of simulation studies that account for relevant biases in the fit procedure and include statistical and systematic uncertainties. The construction of the confidence region bands is shown in Fig. 4. The 90% (95%) confidence level (CL) upper limits are found to be

$$\begin{aligned} \mathcal{B}(B^+ \rightarrow K^+K^+\pi^-) &< 1.1 \times 10^{-8} \quad (1.8 \times 10^{-8}) \text{ at 90\% (95\% CL)} \\ \mathcal{B}(B^+ \rightarrow \pi^+\pi^+K^-) &< 4.6 \times 10^{-8} \quad (5.7 \times 10^{-8}) \text{ at 90\% (95\% CL)} \end{aligned}$$

In summary, searches are presented for the highly-suppressed decays $B^+ \rightarrow K^+K^+\pi^-$ and $B^+ \rightarrow \pi^+\pi^+K^-$ using a data sample of 3.0 fb^{-1} collected by the LHCb experiment in proton–proton collisions at the centre-of-mass energies of 7 and 8 TeV. No evidence is found for these decays and upper limits are placed on $B^+ \rightarrow K^+K^+\pi^-$ and $B^+ \rightarrow \pi^+\pi^+K^-$ branching fractions. The results are approximately fourteen and twenty times more stringent, than previous measurements and constrain various extensions of the SM.

Acknowledgements

We express our gratitude to our colleagues in the CERN accelerator departments for the excellent performance of the LHC. We thank the technical and administrative staff at the LHCb institutes. We acknowledge support from CERN and from the national agencies: CAPES, CNPq, FAPERJ and FINEP (Brazil); NSFC (China); CNRS/IN2P3 (France); BMBF, DFG and MPG (Germany); INFN (Italy); FOM and NWO (The Netherlands); MNiSW and NCN (Poland); MEN/IFA (Romania); MinES and FASO (Russia); MINECO

(Spain); SNSF and SER (Switzerland); NASU (Ukraine); STFC (United Kingdom); NSF (USA). We acknowledge the computing resources that are provided by CERN, IN2P3 (France), KIT and DESY (Germany), INFN (Italy), SURF (The Netherlands), PIC (Spain), GridPP (United Kingdom), RRCKI and Yandex LLC (Russia), CSCS (Switzerland), IFIN-HH (Romania), CBPF (Brazil), PL-GRID (Poland) and OSC (USA). We are indebted to the communities behind the multiple open source software packages on which we depend. Individual groups or members have received support from AvH Foundation (Germany), EPLANET, Marie Skłodowska-Curie Actions and ERC (European Union), Conseil Général de Haute-Savoie, Labex ENIGMASS and OCEVU, Région Auvergne (France), RFBR and Yandex LLC (Russia), GVA, XuntaGal and GENCAT (Spain), Herchel Smith Fund, The Royal Society, Royal Commission for the Exhibition of 1851 and the Leverhulme Trust (United Kingdom).

References

- [1] K. Huitu, D.X. Zhang, C.D. Lu, P. Singer, Searching for new physics in $b \rightarrow s\bar{s}$ decays, Phys. Rev. Lett. 81 (1998) 4313, arXiv:hep-ph/9809566.
- [2] D. Pirjol, J. Zupan, Predictions for $b \rightarrow s\bar{s}$ and $b \rightarrow d\bar{s}$ decays in the SM and with new physics, J. High Energy Phys. 02 (2010) 028, arXiv:0908.3150.
- [3] S. Fajfer, P. Singer, Search for new physics in $\Delta S = 2$ two-body (VV, PP, VP) decays of the B^- meson, Phys. Rev. D 62 (2000) 117702, arXiv:hep-ph/0007132.
- [4] S. Fajfer, J.F. Kamenik, N. Kosnik, $b \rightarrow d\bar{s}$ transition and constraints on new physics in B^- decays, Phys. Rev. D 74 (2006) 034027, arXiv:hep-ph/0605260.
- [5] OPAL Collaboration, G. Abbiendi, et al., Search for new physics in rare B decays, Phys. Lett. B 476 (2000) 233, arXiv:hep-ex/0002008.
- [6] Belle Collaboration, K. Abe, et al., Study of three-body charmless B decays, Phys. Rev. D 65 (2002) 092005, arXiv:hep-ex/0201007.
- [7] BaBar Collaboration, B. Aubert, et al., Measurements of the branching fractions and charge asymmetries of charmless three-body charged B decays, Phys. Rev. Lett. 91 (2003) 051801, arXiv:hep-ex/0304006.
- [8] BaBar Collaboration, B. Aubert, et al., Search for the highly suppressed decays $B^- \rightarrow K^+\pi^-\pi^-$ and $B^- \rightarrow K^-K^-\pi^+$, Phys. Rev. D 78 (2008) 091102, arXiv: 0808.0900.
- [9] LHCb Collaboration, A.A. Alves Jr., et al., The LHCb detector at the LHC, J. Instrum. 3 (2008) S08005.
- [10] LHCb Collaboration, R. Aaij, et al., LHCb detector performance, Int. J. Mod. Phys. A 30 (2015) 1530022, arXiv:1412.6352.
- [11] M. Adinolfi, et al., Performance of the LHCb RICH detector at the LHC, Eur. Phys. J. C 73 (2013) 2431, arXiv:1211.6759.
- [12] A.A. Alves Jr., et al., Performance of the LHCb muon system, J. Instrum. 8 (2013) P02022, arXiv:1211.1346.
- [13] R. Aaij, et al., The LHCb trigger and its performance in 2011, J. Instrum. 8 (2013) P04022, arXiv:1211.3055.
- [14] T. Sjöstrand, S. Mrenna, P. Skands, PYTHIA 6.4 physics and manual, J. High Energy Phys. 05 (2006) 026, arXiv:hep-ph/0603175.
- [15] T. Sjöstrand, S. Mrenna, P. Skands, A brief introduction to PYTHIA 8.1, Comput. Phys. Commun. 178 (2008) 852, arXiv:0710.3820.
- [16] I. Belyaev, et al., Handling of the generation of primary events in Gauss, the LHCb simulation framework, J. Phys. Conf. Ser. 331 (2011) 032047.
- [17] D.J. Lange, The EvtGen particle decay simulation package, Nucl. Instrum. Methods A 462 (2001) 152.
- [18] P. Golonka, Z. Was, PHOTOS Monte Carlo: a precision tool for QED corrections in Z and W decays, Eur. Phys. J. C 45 (2006) 97, arXiv:hep-ph/0506026.
- [19] Geant4 Collaboration, J. Allison, et al., Geant4 developments and applications, IEEE Trans. Nucl. Sci. 53 (2006) 270.
- [20] M. Clemencic, et al., The LHCb simulation application, Gauss: design, evolution and experience, J. Phys. Conf. Ser. 331 (2011) 032023.
- [21] H. Gordon, Searches for CP Violation in $D^+ \rightarrow K^-K^+\pi^+$ Decays at the LHCb Experiment, PhD thesis, Brasenose College, University of Oxford, 2013.
- [22] L. Breiman, J.H. Friedman, R.A. Olshen, C.J. Stone, Classification and Regression Trees, Wadsworth International Group, Belmont, California, USA, 1984.
- [23] R.E. Schapire, Y. Freund, A decision-theoretic generalization of on-line learning and an application to boosting, J. Comput. Syst. Sci. 55 (1997) 119.
- [24] Particle Data Group, K.A. Olive, et al., Review of particle physics, Chin. Phys. C 38 (2014) 090001, and 2015 update.
- [25] G. Punzi, Sensitivity of searches for new signals and its optimization, in: L. Lyons, R. Mount, R. Reitmeyer (Eds.), Statistical Problems in Particle Physics, Astrophysics, and Cosmology, 2003, p. 79, arXiv:physics/0308063.
- [26] T. Skwarnicki, A Study of the Radiative Cascade Transitions between the Upsilon-prime and Upsilon Resonances, PhD thesis, Institute of Nuclear Physics, Krakow, 1986, DESY-F31-86-02.
- [27] ARGUS Collaboration, H. Albrecht, et al., Exclusive hadronic decays of B mesons, Z. Phys. C 48 (1990) 543.
- [28] L. Anderlini, et al., The PIDCalib Package, Tech. Rep. LHCb-PUB-2016-021, CERN-LHCb-PUB-2016-021, CERN, Geneva, Jul. 2016.
- [29] Belle Collaboration, A. Garmash, et al., Evidence for large direct CP violation in $B^\pm \rightarrow \rho(770)^0 K^\pm$ from analysis of the three-body charmless $B^\pm \rightarrow K^\pm \pi^\pm \pi^\mp$ decay, Phys. Rev. Lett. 96 (2006) 251803, arXiv:hep-ex/0512066.
- [30] BaBar Collaboration, B. Aubert, et al., Evidence for direct CP violation from Dalitz-plot analysis of $B^\pm \rightarrow K^\pm \pi^\mp \pi^\pm$, Phys. Rev. D 78 (2008) 012004, arXiv: 0803.4451.
- [31] BaBar Collaboration, B. Aubert, et al., Observation of the decay $B^+ \rightarrow K^+K^-\pi^+$, Phys. Rev. Lett. 99 (2007) 221801, arXiv:0708.0376.
- [32] G.J. Feldman, R.D. Cousins, A unified approach to the classical statistical analysis of small signals, Phys. Rev. D 57 (1998) 3873, arXiv:physics/9711021.

LHCb Collaboration

R. Aaij³⁹, B. Adeva³⁸, M. Adinolfi⁴⁷, Z. Ajaltouni⁵, S. Akar⁶, J. Albrecht¹⁰, F. Alessio³⁹, M. Alexander⁵², S. Ali⁴², G. Alkhazov³¹, P. Alvarez Cartelle⁵⁴, A.A. Alves Jr.⁵⁸, S. Amato², S. Amerio²³, Y. Amhis⁷, L. An⁴⁰, L. Anderlini¹⁸, G. Andreassi⁴⁰, M. Andreotti^{17,g}, J.E. Andrews⁵⁹, R.B. Appleby⁵⁵, O. Aquines Gutierrez¹¹, F. Archilli¹, P. d'Argent¹², J. Arnau Romeu⁶, A. Artamonov³⁶, M. Artuso⁶⁰, E. Aslanides⁶, G. Auriemma^{26,s}, M. Baalouch⁵, I. Babuschkin⁵⁵, S. Bachmann¹², J.J. Back⁴⁹, A. Badalov³⁷, C. Baesso⁶¹, W. Baldini¹⁷, R.J. Barlow⁵⁵, C. Barschel³⁹, S. Barsuk⁷, W. Barter³⁹, V. Batozskaya²⁹, B. Batsukh⁶⁰, V. Battista⁴⁰, A. Bay⁴⁰, L. Beaucourt⁴, J. Beddow⁵², F. Bedeschi²⁴, I. Bediaga¹, L.J. Bel⁴², V. Bellee⁴⁰, N. Belloli^{21,i}, K. Belous³⁶, I. Belyaev³², E. Ben-Haim⁸, G. Bencivenni¹⁹, S. Benson³⁹, J. Benton⁴⁷, A. Berezhnoy³³, R. Bernet⁴¹, A. Bertolin²³, F. Betti¹⁵, M.-O. Bettler³⁹, M. van Beuzekom⁴², S. Bifani⁴⁶, P. Billoir⁸, T. Bird⁵⁵, A. Birnkraut¹⁰, A. Bitadze⁵⁵, A. Bizzeti^{18,u}, T. Blake⁴⁹, F. Blanc⁴⁰, J. Blouw¹¹, S. Blusk⁶⁰, V. Bocci²⁶, T. Boettcher⁵⁷, A. Bondar³⁵, N. Bondar^{31,39}, W. Bonivento¹⁶, A. Borgheresi^{21,i}, S. Borghi⁵⁵, M. Borisyan⁶⁷, M. Borsato³⁸, F. Bossu⁷, M. Bouabdil⁹, T.J.V. Bowcock⁵³, E. Bowen⁴¹, C. Bozzi^{17,39}, S. Braun¹², M. Britsch¹², T. Britton⁶⁰, J. Brodzicka⁵⁵, E. Buchanan⁴⁷, C. Burr⁵⁵, A. Bursche², J. Buytaert³⁹, S. Cadeddu¹⁶, R. Calabrese^{17,g}, M. Calvi^{21,i}, M. Calvo Gomez^{37,m}, A. Camboni³⁷, P. Campana¹⁹, D. Campora Perez³⁹, D.H. Campora Perez³⁹, L. Capriotti⁵⁵, A. Carbone^{15,e}, G. Carboni^{25,j}, R. Cardinale^{20,h}, A. Cardini¹⁶, P. Carniti^{21,i}, L. Carson⁵¹, K. Carvalho Akiba², G. Casse⁵³, L. Cassina^{21,i}, L. Castillo Garcia⁴⁰, M. Cattaneo³⁹, Ch. Cauet¹⁰, G. Cavallero²⁰, R. Cenci^{24,t}, M. Charles⁸, Ph. Charpentier³⁹, G. Chatzikonstantinidis⁴⁶, M. Chefdeville⁴, S. Chen⁵⁵, S.-F. Cheung⁵⁶,

- V. Chobanova ³⁸, M. Chrzaszcz ^{41,27}, X. Cid Vidal ³⁸, G. Ciezarek ⁴², P.E.L. Clarke ⁵¹, M. Clemencic ³⁹, H.V. Cliff ⁴⁸, J. Closier ³⁹, V. Coco ⁵⁸, J. Cogan ⁶, E. Cogneras ⁵, V. Cogoni ^{16,f}, L. Cojocariu ³⁰, G. Collazuol ^{23,o}, P. Collins ³⁹, A. Comerma-Montells ¹², A. Contu ³⁹, A. Cook ⁴⁷, S. Coquereau ⁸, G. Corti ³⁹, M. Corvo ^{17,g}, C.M. Costa Sobral ⁴⁹, B. Couturier ³⁹, G.A. Cowan ⁵¹, D.C. Craik ⁵¹, A. Crocombe ⁴⁹, M. Cruz Torres ⁶¹, S. Cunliffe ⁵⁴, R. Currie ⁵⁴, C. D'Ambrosio ³⁹, E. Dall'Occo ⁴², J. Dalseno ⁴⁷, P.N.Y. David ⁴², A. Davis ⁵⁸, O. De Aguiar Francisco ², K. De Bruyn ⁶, S. De Capua ⁵⁵, M. De Cian ¹², J.M. De Miranda ¹, L. De Paula ², M. De Serio ^{14,d}, P. De Simone ¹⁹, C.-T. Dean ⁵², D. Decamp ⁴, M. Deckenhoff ¹⁰, L. Del Buono ⁸, M. Demmer ¹⁰, D. Derkach ⁶⁷, O. Deschamps ⁵, F. Dettori ³⁹, B. Dey ²², A. Di Canto ³⁹, H. Dijkstra ³⁹, F. Dordei ³⁹, M. Dorigo ⁴⁰, A. Dosil Suárez ³⁸, A. Dovbnya ⁴⁴, K. Dreimanis ⁵³, L. Dufour ⁴², G. Dujany ⁵⁵, K. Dungs ³⁹, P. Durante ³⁹, R. Dzhelyadin ³⁶, A. Dziurda ³⁹, A. Dzyuba ³¹, N. Déléage ⁴, S. Easo ⁵⁰, M. Ebert ⁵¹, U. Egede ⁵⁴, V. Egorychev ³², S. Eidelman ³⁵, S. Eisenhardt ⁵¹, U. Eitschberger ¹⁰, R. Ekelhof ¹⁰, L. Eklund ⁵², Ch. Elsasser ⁴¹, S. Ely ⁶⁰, S. Esen ¹², H.M. Evans ⁴⁸, T. Evans ⁵⁶, A. Falabella ¹⁵, N. Farley ⁴⁶, S. Farry ⁵³, R. Fay ⁵³, D. Fazzini ^{21,i}, D. Ferguson ⁵¹, V. Fernandez Albor ³⁸, A. Fernandez Prieto ³⁸, F. Ferrari ^{15,39}, F. Ferreira Rodrigues ¹, M. Ferro-Luzzi ³⁹, S. Filippov ³⁴, M. Fiore ^{17,g}, M. Fiorini ^{17,g}, M. Firlej ²⁸, C. Fitzpatrick ⁴⁰, T. Fiutowski ²⁸, F. Fleuret ^{7,b}, K. Fohl ³⁹, M. Fontana ¹⁶, F. Fontanelli ^{20,h}, D.C. Forshaw ⁶⁰, R. Forty ³⁹, M. Frank ³⁹, C. Frei ³⁹, J. Fu ^{22,q}, E. Furfarò ^{25,j}, C. Färber ³⁹, A. Gallas Torreira ³⁸, D. Galli ^{15,e}, S. Gallorini ²³, S. Gambetta ⁵¹, M. Gandelman ², P. Gandini ⁵⁶, Y. Gao ³, L.M. Garcia Martin ⁶⁸, J. García Pardiñas ³⁸, J. Garra Tico ⁴⁸, L. Garrido ³⁷, P.J. Garsed ⁴⁸, D. Gascon ³⁷, C. Gaspar ³⁹, L. Gavardi ¹⁰, G. Gazzoni ⁵, D. Gerick ¹², E. Gersabeck ¹², M. Gersabeck ⁵⁵, T. Gershon ⁴⁹, Ph. Ghez ⁴, S. Gianì ⁴⁰, V. Gibson ⁴⁸, O.G. Girard ⁴⁰, L. Giubega ³⁰, K. Gizdov ⁵¹, V.V. Gligorov ⁸, D. Golubkov ³², A. Golutvin ^{54,39}, A. Gomes ^{1,a}, I.V. Gorelov ³³, C. Gotti ^{21,i}, M. Grabalosa Gándara ⁵, R. Graciani Diaz ³⁷, L.A. Granado Cardoso ³⁹, E. Graugés ³⁷, E. Graverini ⁴¹, G. Graziani ¹⁸, A. Grecu ³⁰, P. Griffith ⁴⁶, L. Grillo ¹², B.R. Gruberg Cazon ⁵⁶, O. Grünberg ⁶⁵, E. Gushchin ³⁴, Yu. Guz ³⁶, T. Gys ³⁹, C. Göbel ⁶¹, T. Hadavizadeh ⁵⁶, C. Hadjivassiliou ⁶⁰, G. Haefeli ⁴⁰, C. Haen ³⁹, S.C. Haines ⁴⁸, S. Hall ⁵⁴, B. Hamilton ⁵⁹, X. Han ¹², S. Hansmann-Menzemer ¹², N. Harnew ⁵⁶, S.T. Harnew ⁴⁷, J. Harrison ⁵⁵, M. Hatch ³⁹, J. He ⁶², T. Head ⁴⁰, A. Heister ⁹, K. Hennessy ⁵³, P. Henrard ⁵, L. Henry ⁸, J.A. Hernando Morata ³⁸, E. van Herwijnen ³⁹, M. Heß ⁶⁵, A. Hicheur ², D. Hill ⁵⁶, C. Hombach ⁵⁵, W. Hulsbergen ⁴², T. Humair ⁵⁴, M. Hushchyn ⁶⁷, N. Hussain ⁵⁶, D. Hutchcroft ⁵³, M. Idzik ²⁸, P. Ilten ⁵⁷, R. Jacobsson ³⁹, A. Jaeger ¹², J. Jalocha ⁵⁶, E. Jans ⁴², A. Jawahery ⁵⁹, M. John ⁵⁶, D. Johnson ³⁹, C.R. Jones ⁴⁸, C. Joram ³⁹, B. Jost ³⁹, N. Jurik ⁶⁰, S. Kandybei ⁴⁴, W. Kanso ⁶, M. Karacson ³⁹, J.M. Kariuki ⁴⁷, S. Kärodia ⁵², M. Kecke ¹², M. Kelsey ⁶⁰, I.R. Kenyon ⁴⁶, M. Kenzie ³⁹, T. Ketel ⁴³, E. Khairullin ⁶⁷, B. Khanji ^{21,39,i}, C. Khurewathanakul ⁴⁰, T. Kirn ⁹, S. Klaver ⁵⁵, K. Klimaszewski ²⁹, S. Koliiev ⁴⁵, M. Kolpin ¹², I. Komarov ⁴⁰, R.F. Koopman ⁴³, P. Koppenburg ⁴², A. Kozachuk ³³, M. Kozeiha ⁵, L. Kravchuk ³⁴, K. Kreplin ¹², M. Kreps ⁴⁹, P. Krokovny ³⁵, F. Kruse ¹⁰, W. Krzemien ²⁹, W. Kucewicz ^{27,l}, M. Kucharczyk ²⁷, V. Kudryavtsev ³⁵, A.K. Kuonen ⁴⁰, K. Kurek ²⁹, T. Kvaratskheliya ^{32,39}, D. Lacarrere ³⁹, G. Lafferty ^{55,39}, A. Lai ¹⁶, D. Lambert ⁵¹, G. Lanfranchi ¹⁹, C. Langenbruch ⁹, B. Langhans ³⁹, T. Latham ⁴⁹, C. Lazzeroni ⁴⁶, R. Le Gac ⁶, J. van Leerdam ⁴², J.-P. Lees ⁴, A. Leflat ^{33,39}, J. Lefrançois ⁷, R. Lefèvre ⁵, F. Lemaitre ³⁹, E. Lemos Cid ³⁸, O. Leroy ⁶, T. Lesiak ²⁷, B. Leverington ¹², Y. Li ⁷, T. Likhomanenko ^{67,66}, R. Lindner ³⁹, C. Linn ³⁹, F. Lionetto ⁴¹, B. Liu ¹⁶, X. Liu ³, D. Loh ⁴⁹, I. Longstaff ⁵², J.H. Lopes ², D. Lucchesi ^{23,o}, M. Lucio Martinez ³⁸, H. Luo ⁵¹, A. Lupato ²³, E. Luppi ^{17,g}, O. Lupton ⁵⁶, A. Lusiani ²⁴, X. Lyu ⁶², F. Machefert ⁷, F. Maciuc ³⁰, O. Maev ³¹, K. Maguire ⁵⁵, S. Malde ⁵⁶, A. Malinin ⁶⁶, T. Maltsev ³⁵, G. Manca ⁷, G. Mancinelli ⁶, P. Manning ⁶⁰, J. Maratas ⁵, J.F. Marchand ⁴, U. Marconi ¹⁵, C. Marin Benito ³⁷, P. Marino ^{24,t}, J. Marks ¹², G. Martellotti ²⁶, M. Martin ⁶, M. Martinelli ⁴⁰, D. Martinez Santos ³⁸, F. Martinez Vidal ⁶⁸, D. Martins Tostes ², L.M. Massacrier ⁷, A. Massafferri ¹, R. Matev ³⁹, A. Mathad ⁴⁹, Z. Mathe ³⁹, C. Matteuzzi ²¹, A. Mauri ⁴¹, B. Maurin ⁴⁰, A. Mazurov ⁴⁶, M. McCann ⁵⁴, J. McCarthy ⁴⁶, A. McNab ⁵⁵, R. McNulty ¹³, B. Meadows ⁵⁸, F. Meier ¹⁰, M. Meissner ¹², D. Melnychuk ²⁹, M. Merk ⁴², A. Merli ^{22,q}, E. Michielin ²³, D.A. Milanes ⁶⁴, M.-N. Minard ⁴, D.S. Mitzel ¹², J. Molina Rodriguez ⁶¹, I.A. Monroy ⁶⁴, S. Monteil ⁵, M. Morandin ²³, P. Morawski ²⁸, A. Mordà ⁶, M.J. Morello ^{24,t}, J. Moron ²⁸, A.B. Morris ⁵¹, R. Mountain ⁶⁰, F. Muheim ⁵¹, M. Mulder ⁴², M. Mussini ¹⁵, D. Müller ⁵⁵, J. Müller ¹⁰, K. Müller ⁴¹, V. Müller ¹⁰, P. Naik ⁴⁷, T. Nakada ⁴⁰, R. Nandakumar ^{50,*}, A. Nandi ⁵⁶, I. Nasteva ², M. Needham ⁵¹, N. Neri ²², S. Neubert ¹², N. Neufeld ³⁹, M. Neuner ¹², A.D. Nguyen ⁴⁰, C. Nguyen-Mau ^{40,n}, S. Nieswand ⁹, R. Niet ¹⁰, N. Nikitin ³³, T. Nikodem ¹², A. Novoselov ³⁶, D.P. O'Hanlon ⁴⁹,

- A. Oblakowska-Mucha ²⁸, V. Obraztsov ³⁶, S. Ogilvy ¹⁹, R. Oldeman ⁴⁸, C.J.G. Onderwater ⁶⁹,
 J.M. Otalora Goicochea ², A. Otto ³⁹, P. Owen ⁴¹, A. Oyanguren ⁶⁸, P.R. Pais ⁴⁰, A. Palano ^{14,d},
 F. Palombo ^{22,q}, M. Palutan ¹⁹, J. Panman ³⁹, A. Papanestis ⁵⁰, M. Pappagallo ⁵², L.L. Pappalardo ^{17,g},
 C. Pappeneheimer ⁵⁸, W. Parker ⁵⁹, C. Parkes ⁵⁵, G. Passaleva ¹⁸, G.D. Patel ⁵³, M. Patel ⁵⁴, C. Patrignani ^{15,e},
 A. Pearce ^{55,50}, A. Pellegrino ⁴², G. Penso ^{26,k}, M. Pepe Altarelli ³⁹, S. Perazzini ³⁹, P. Perret ⁵,
 L. Pescatore ⁴⁶, K. Petridis ⁴⁷, A. Petrolini ^{20,h}, A. Petrov ⁶⁶, M. Petruzzo ^{22,q}, E. Picatoste Olloqui ³⁷,
 B. Pietrzyk ⁴, M. Pikies ²⁷, D. Pinci ²⁶, A. Pistone ²⁰, A. Piucci ¹², S. Playfer ⁵¹, M. Plo Casasus ³⁸,
 T. Poikela ³⁹, F. Polci ⁸, A. Poluektov ^{49,35}, I. Polyakov ³², E. Polycarpo ², G.J. Pomery ⁴⁷, A. Popov ³⁶,
 D. Popov ^{11,39}, B. Popovici ³⁰, C. Potterat ², E. Price ⁴⁷, J.D. Price ⁵³, J. Prisciandaro ³⁸, A. Pritchard ⁵³,
 C. Prouve ⁴⁷, V. Pugatch ⁴⁵, A. Puig Navarro ⁴⁰, G. Punzi ^{24,p}, W. Qian ⁵⁶, R. Quagliani ^{7,47}, B. Rachwal ²⁷,
 J.H. Rademacker ⁴⁷, M. Rama ²⁴, M. Ramos Pernas ³⁸, M.S. Rangel ², I. Raniuk ⁴⁴, G. Raven ⁴³, F. Redi ⁵⁴,
 S. Reichert ¹⁰, A.C. dos Reis ¹, C. Remon Alepuz ⁶⁸, V. Renaudin ⁷, S. Ricciardi ⁵⁰, S. Richards ⁴⁷, M. Rihl ³⁹,
 K. Rinnert ^{53,39}, V. Rives Molina ³⁷, P. Robbe ^{7,39}, A.B. Rodrigues ¹, E. Rodrigues ⁵⁸, J.A. Rodriguez Lopez ⁶⁴,
 P. Rodriguez Perez ⁵⁵, A. Rogozhnikov ⁶⁷, S. Roiser ³⁹, V. Romanovskiy ³⁶, A. Romero Vidal ³⁸,
 J.W. Ronayne ¹³, M. Rotondo ²³, T. Ruf ³⁹, P. Ruiz Valls ⁶⁸, J.J. Saborido Silva ³⁸, E. Sadykhov ³²,
 N. Sagidova ³¹, B. Saitta ^{16,f}, V. Salustino Guimaraes ², C. Sanchez Mayordomo ⁶⁸, B. Sanmartin Sedes ³⁸,
 R. Santacesaria ²⁶, C. Santamarina Rios ³⁸, M. Santimaria ¹⁹, E. Santovetti ^{25,j}, A. Sarti ^{19,k}, C. Satriano ^{26,s},
 A. Satta ²⁵, D.M. Saunders ⁴⁷, D. Savrina ^{32,33}, S. Schael ⁹, M. Schiller ³⁹, H. Schindler ³⁹, M. Schlupp ¹⁰,
 M. Schmelling ¹¹, T. Schmelzer ¹⁰, B. Schmidt ³⁹, O. Schneider ⁴⁰, A. Schopper ³⁹, M. Schubiger ⁴⁰,
 M.-H. Schune ⁷, R. Schwemmer ³⁹, B. Sciascia ¹⁹, A. Sciubba ^{26,k}, A. Semennikov ³², A. Sergi ⁴⁶, N. Serra ⁴¹,
 J. Serrano ⁶, L. Sestini ²³, P. Seyfert ²¹, M. Shapkin ³⁶, I. Shapoval ^{17,44,g}, Y. Shcheglov ³¹, T. Shears ⁵³,
 L. Shekhtman ³⁵, V. Shevchenko ⁶⁶, A. Shires ¹⁰, B.G. Siddi ¹⁷, R. Silva Coutinho ⁴¹, L. Silva de Oliveira ²,
 G. Simi ^{23,o}, S. Simone ^{14,d}, M. Sirendi ⁴⁸, N. Skidmore ⁴⁷, T. Skwarnicki ⁶⁰, E. Smith ⁵⁴, I.T. Smith ⁵¹,
 J. Smith ⁴⁸, M. Smith ⁵⁵, H. Snoek ⁴², M.D. Sokoloff ⁵⁸, F.J.P. Soler ⁵², D. Souza ⁴⁷, B. Souza De Paula ²,
 B. Spaan ¹⁰, P. Spradlin ⁵², S. Sridharan ³⁹, F. Stagni ³⁹, M. Stahl ¹², S. Stahl ³⁹, P. Steffko ⁴⁰, S. Stefkova ⁵⁴,
 O. Steinkamp ⁴¹, O. Stenyakin ³⁶, S. Stevenson ⁵⁶, S. Stoica ³⁰, S. Stone ⁶⁰, B. Storaci ⁴¹, S. Stracka ^{24,t},
 M. Straticiuc ³⁰, U. Straumann ⁴¹, L. Sun ⁵⁸, W. Sutcliffe ⁵⁴, K. Swientek ²⁸, V. Syropoulos ⁴³,
 M. Szczekowski ²⁹, T. Szumlak ²⁸, S. T'Jampens ⁴, A. Tayduganov ⁶, T. Tekampe ¹⁰, G. Tellarini ^{17,g},
 F. Teubert ³⁹, C. Thomas ⁵⁶, E. Thomas ³⁹, J. van Tilburg ⁴², V. Tisserand ⁴, M. Tobin ⁴⁰, S. Tolk ⁴⁸,
 L. Tomassetti ^{17,g}, D. Tonelli ³⁹, S. Topp-Joergensen ⁵⁶, F. Toriello ⁶⁰, E. Tournefier ⁴, S. Tourneur ⁴⁰,
 K. Trabelsi ⁴⁰, M. Traill ⁵², M.T. Tran ⁴⁰, M. Tresch ⁴¹, A. Trisovic ³⁹, A. Tsaregorodtsev ⁶, P. Tsopelas ⁴²,
 A. Tully ⁴⁸, N. Tuning ⁴², A. Ukleja ²⁹, A. Ustyuzhanin ^{67,66}, U. Uwer ¹², C. Vacca ^{16,39,f}, V. Vagnoni ^{15,39},
 S. Valat ³⁹, G. Valenti ¹⁵, A. Vallier ⁷, R. Vazquez Gomez ¹⁹, P. Vazquez Regueiro ³⁸, S. Vecchi ¹⁷,
 M. van Veghel ⁴², J.J. Velthuis ⁴⁷, M. Veltri ^{18,r}, G. Veneziano ⁴⁰, A. Venkateswaran ⁶⁰, M. Vesterinen ¹²,
 B. Viaud ⁷, D. Vieira ¹, M. Vieites Diaz ³⁸, X. Vilasis-Cardona ^{37,m}, V. Volkov ³³, A. Vollhardt ⁴¹, B. Voneki ³⁹,
 D. Voong ⁴⁷, A. Vorobyev ³¹, V. Vorobyev ³⁵, C. Voß ⁶⁵, J.A. de Vries ⁴², C. Vázquez Sierra ³⁸, R. Waldi ⁶⁵,
 C. Wallace ⁴⁹, R. Wallace ¹³, J. Walsh ²⁴, J. Wang ⁶⁰, D.R. Ward ⁴⁸, H.M. Wark ⁵³, N.K. Watson ⁴⁶,
 D. Websdale ⁵⁴, A. Weiden ⁴¹, M. Whitehead ³⁹, J. Wicht ⁴⁹, G. Wilkinson ^{56,39}, M. Wilkinson ⁶⁰,
 M. Williams ³⁹, M.P. Williams ⁴⁶, M. Williams ⁵⁷, T. Williams ⁴⁶, F.F. Wilson ^{50,*}, J. Wimberley ⁵⁹,
 J. Wishahi ¹⁰, W. Wislicki ²⁹, M. Witek ²⁷, G. Wormser ⁷, S.A. Wotton ⁴⁸, K. Wraight ⁵², S. Wright ⁴⁸,
 K. Wyllie ³⁹, Y. Xie ⁶³, Z. Xing ⁶⁰, Z. Xu ⁴⁰, Z. Yang ³, H. Yin ⁶³, J. Yu ⁶³, X. Yuan ³⁵, O. Yushchenko ³⁶,
 M. Zangoli ¹⁵, K.A. Zarebski ⁴⁶, M. Zavertyaev ^{11,c}, L. Zhang ³, Y. Zhang ⁷, Y. Zhang ⁶², A. Zhelezov ¹²,
 Y. Zheng ⁶², A. Zhokhov ³², X. Zhu ³, V. Zhukov ⁹, S. Zucchelli ¹⁵

¹ Centro Brasileiro de Pesquisas Físicas (CBPF), Rio de Janeiro, Brazil² Universidade Federal do Rio de Janeiro (UFRJ), Rio de Janeiro, Brazil³ Center for High Energy Physics, Tsinghua University, Beijing, China⁴ LAPP, Université Savoie Mont-Blanc, CNRS/IN2P3, Annecy-Le-Vieux, France⁵ Clermont Université, Université Blaise Pascal, CNRS/IN2P3, LPC, Clermont-Ferrand, France⁶ CPPM, Aix-Marseille Université, CNRS/IN2P3, Marseille, France⁷ LAL, Université Paris-Sud, CNRS/IN2P3, Orsay, France⁸ LPNHE, Université Pierre et Marie Curie, Université Paris Diderot, CNRS/IN2P3, Paris, France⁹ I. Physikalisches Institut, RWTH Aachen University, Aachen, Germany¹⁰ Fakultät Physik, Technische Universität Dortmund, Dortmund, Germany¹¹ Max-Planck-Institut für Kernphysik (MPIK), Heidelberg, Germany¹² Physikalisches Institut, Ruprecht-Karls-Universität Heidelberg, Heidelberg, Germany¹³ School of Physics, University College Dublin, Dublin, Ireland

- ¹⁴ Sezione INFN di Bari, Bari, Italy
¹⁵ Sezione INFN di Bologna, Bologna, Italy
¹⁶ Sezione INFN di Cagliari, Cagliari, Italy
¹⁷ Sezione INFN di Ferrara, Ferrara, Italy
¹⁸ Sezione INFN di Firenze, Firenze, Italy
¹⁹ Laboratori Nazionali dell'INFN di Frascati, Frascati, Italy
²⁰ Sezione INFN di Genova, Genova, Italy
²¹ Sezione INFN di Milano Bicocca, Milano, Italy
²² Sezione INFN di Milano, Milano, Italy
²³ Sezione INFN di Padova, Padova, Italy
²⁴ Sezione INFN di Pisa, Pisa, Italy
²⁵ Sezione INFN di Roma Tor Vergata, Roma, Italy
²⁶ Sezione INFN di Roma La Sapienza, Roma, Italy
²⁷ Henryk Niewodniczanski Institute of Nuclear Physics Polish Academy of Sciences, Kraków, Poland
²⁸ AGH – University of Science and Technology, Faculty of Physics and Applied Computer Science, Kraków, Poland
²⁹ National Center for Nuclear Research (NCBJ), Warsaw, Poland
³⁰ Horia Hulubei National Institute of Physics and Nuclear Engineering, Bucharest-Magurele, Romania
³¹ Petersburg Nuclear Physics Institute (PNPI), Gatchina, Russia
³² Institute of Theoretical and Experimental Physics (ITEP), Moscow, Russia
³³ Institute of Nuclear Physics, Moscow State University (SINP MSU), Moscow, Russia
³⁴ Institute for Nuclear Research of the Russian Academy of Sciences (INR RAN), Moscow, Russia
³⁵ Budker Institute of Nuclear Physics (SB RAS) and Novosibirsk State University, Novosibirsk, Russia
³⁶ Institute for High Energy Physics (IHEP), Protvino, Russia
³⁷ Universitat de Barcelona, Barcelona, Spain
³⁸ Universidad de Santiago de Compostela, Santiago de Compostela, Spain
³⁹ European Organization for Nuclear Research (CERN), Geneva, Switzerland
⁴⁰ Ecole Polytechnique Fédérale de Lausanne (EPFL), Lausanne, Switzerland
⁴¹ Physik-Institut, Universität Zürich, Zürich, Switzerland
⁴² Nikhef National Institute for Subatomic Physics, Amsterdam, The Netherlands
⁴³ Nikhef National Institute for Subatomic Physics and VU University Amsterdam, Amsterdam, The Netherlands
⁴⁴ NSC Kharkiv Institute of Physics and Technology (NSC KIPT), Kharkiv, Ukraine
⁴⁵ Institute for Nuclear Research of the National Academy of Sciences (KINR), Kyiv, Ukraine
⁴⁶ University of Birmingham, Birmingham, United Kingdom
⁴⁷ H.H. Wills Physics Laboratory, University of Bristol, Bristol, United Kingdom
⁴⁸ Cavendish Laboratory, University of Cambridge, Cambridge, United Kingdom
⁴⁹ Department of Physics, University of Warwick, Coventry, United Kingdom
⁵⁰ STFC Rutherford Appleton Laboratory, Didcot, United Kingdom
⁵¹ School of Physics and Astronomy, University of Edinburgh, Edinburgh, United Kingdom
⁵² School of Physics and Astronomy, University of Glasgow, Glasgow, United Kingdom
⁵³ Oliver Lodge Laboratory, University of Liverpool, Liverpool, United Kingdom
⁵⁴ Imperial College London, London, United Kingdom
⁵⁵ School of Physics and Astronomy, University of Manchester, Manchester, United Kingdom
⁵⁶ Department of Physics, University of Oxford, Oxford, United Kingdom
⁵⁷ Massachusetts Institute of Technology, Cambridge, MA, United States
⁵⁸ University of Cincinnati, Cincinnati, OH, United States
⁵⁹ University of Maryland, College Park, MD, United States
⁶⁰ Syracuse University, Syracuse, NY, United States
⁶¹ Pontifícia Universidade Católica do Rio de Janeiro (PUC-Rio), Rio de Janeiro, Brazil ^v
⁶² University of Chinese Academy of Sciences, Beijing, China ^w
⁶³ Institute of Particle Physics, Central China Normal University, Wuhan, Hubei, China ^w
⁶⁴ Departamento de Física, Universidad Nacional de Colombia, Bogota, Colombia ^x
⁶⁵ Institut für Physik, Universität Rostock, Rostock, Germany ^y
⁶⁶ National Research Centre Kurchatov Institute, Moscow, Russia ^z
⁶⁷ Yandex School of Data Analysis, Moscow, Russia ^z
⁶⁸ Instituto de Física Corpuscular (IFIC), Universitat de València-CSIC, Valencia, Spain ^{aa}
⁶⁹ Van Swinderen Institute, University of Groningen, Groningen, The Netherlands ^{ab}

* Corresponding author.

E-mail address: raja.nandakumar@cern.ch (R. Nandakumar).

^a Universidade Federal do Triângulo Mineiro (UFTM), Uberaba-MG, Brazil.

^b Laboratoire Leprince-Ringuet, Palaiseau, France.

^c P.N. Lebedev Physical Institute, Russian Academy of Science (LPI RAS), Moscow, Russia.

^d Università di Bari, Bari, Italy.

^e Università di Bologna, Bologna, Italy.

^f Università di Cagliari, Cagliari, Italy.

^g Università di Ferrara, Ferrara, Italy.

^h Università di Genova, Genova, Italy.

ⁱ Università di Milano Bicocca, Milano, Italy.

^j Università di Roma Tor Vergata, Roma, Italy.

^k Università di Roma La Sapienza, Roma, Italy.

^l AGH – University of Science and Technology, Faculty of Computer Science, Electronics and Telecommunications, Kraków, Poland.

^m LIFAELS, La Salle, Universitat Ramon Llull, Barcelona, Spain.

ⁿ Hanoi University of Science, Hanoi, Viet Nam.

^o Università di Padova, Padova, Italy.

^p Università di Pisa, Pisa, Italy.

^q Università degli Studi di Milano, Milano, Italy.

^r Università di Urbino, Urbino, Italy.

^s Università della Basilicata, Potenza, Italy.

^t Scuola Normale Superiore, Pisa, Italy.

^u Università di Modena e Reggio Emilia, Modena, Italy.

^v Associated to Universidade Federal do Rio de Janeiro (UFRJ), Rio de Janeiro, Brazil.

^w Associated to Center for High Energy Physics, Tsinghua University, Beijing, China.

^x Associated to LPNHE, Université Pierre et Marie Curie, Université Paris Diderot, CNRS/IN2P3, Paris, France.

^y Associated to Physikalisches Institut, Ruprecht-Karls-Universität Heidelberg, Heidelberg, Germany.

^z Associated to Institute of Theoretical and Experimental Physics (ITEP), Moscow, Russia.

^{aa} Associated to Universitat de Barcelona, Barcelona, Spain.

^{ab} Associated to Nikhef National Institute for Subatomic Physics, Amsterdam, The Netherlands.